J Physiol Biochem (2017) 73:561–573
DOI 10.1007/s13105-017-0587-8

ORIGINAL ARTICLE

Molecular analysis of oxalate-induced endoplasmic reticulum stress mediated apoptosis in the pathogenesis of kidney stone disease

Albert Abhishek[1] · Shaly Benita[1] · Monika Kumari[1] · Divya Ganesan[1] · Eldho Paul[1] · Ponnusamy Sasikumar[2] · Ayyavu Mahesh[3] · Subramani Yuvaraj[1] · Tharmarajan Ramprasath[4] · Govindan Sadasivam Selvam[1,5]

Received: 24 February 2017 / Accepted: 25 August 2017 / Published online: 5 September 2017

Abstract Oxalate, a non-essential end product of metabolism, causes hyperoxaluria and eventually calcium oxalate (CaOx) stone disease. Kidney cells exposed to oxalate stress results in generation of reactive oxygen species (ROS) and progression of stone formation. Perturbations in endoplasmic reticulum (ER) result in accumulation of misfolded proteins and Ca^{2+} ions homeostasis imbalance and serve as a common pathway for various diseases, including kidney disorders. ER stress induces up-regulation of pro-survival protein glucose-regulated protein 78 (GRP78) and pro-apoptotic signaling protein C/EBP homologous protein (CHOP). Since the association of oxalate toxicity and ER stress on renal cell damage is uncertain, the present study is an attempt to elucidate the interaction of GRP78 with oxalate by computational analysis and study the role of ER stress in oxalate-mediated apoptosis in vitro and in vivo. Molecular docking results showed that GRP78-oxalate/CaOx interaction takes place. Oxalate stress significantly up-regulated expression of ER stress markers GRP78 and CHOP both in vitro and in vivo. Exposure of oxalate increased ROS generation and altered antioxidant enzyme activities. *N*-Acetyl cysteine treatment significantly ameliorated oxalate-mediated oxidative stress and moderately attenuated ER stress marker expression. The result indicates oxalate toxicity initiated oxidative stress-induced ER stress and also activating ER stress mediated apoptosis directly. In addition, the up-regulation of transforming growth factor β-$_1$ revealed oxalate may induce kidney fibrosis through ER stress-mediated mechanisms. The present study provide insights into the pathogenic role of oxidative and ER stress by oxalate exposure in the formation of calcium oxalate stone.

Keywords ER stress · Oxidative stress · Calcium oxalate · CHOP · GRP78 · Renal fibrosis

✉ Govindan Sadasivam Selvam
drselvamgsbiochem@rediffmail.com;
drselvamgsbiochem@yahoo.com

[1] Department of Biochemistry, Centre for Excellence in Genomics Science, School of Biological Sciences, Madurai Kamaraj University, Madurai 625 021, India

[2] Department of Oral Biology, School of Dental Medicine, University at Buffalo, Buffalo, NY, USA

[3] DBT-IPLS Programme, School of Biological Sciences, Madurai Kamaraj University, Madurai 625 021, India

[4] Center for Molecular and Translational Medicine, Georgia State University, Atlanta, GA, USA

[5] Department of Biochemistry, Centre for Advanced Studies in Functional Genomics, School of Biological Sciences, Madurai Kamaraj University, Madurai 625 021, India

Introduction

Urolithiasis is a multifactorial process influenced by genetic and environmental factors [31]. Oxalate is the major risk factor for kidney stone formation and accounts for the key crystalline composition of nephrolithiasis. The interaction of renal cells with oxalate ions act as a precursor for cell injury and subsequently, the cells undergo apoptosis initiating a cascade of events leading to further crystallization, crystal retention, and development of stone nidi. Crystallization occurs as a result of crystal binding sites that allow crystal deposition and stone formation [16]. However, the underlining factor for calcium oxalate (CaOx) stone formation is not clear [4].

Interactions between the oxalate/crystals and renal cells result in generation of reactive oxygen species (ROS) that subsequently leads to decrease in antioxidant capacity, renal injury, and inflammation [8, 15]. Persistent oxidative stress conditions promote misfolded and unfolded protein

accumulation in the endoplasmic reticulum (ER) lumen indicating ER stress and ROS generation are closely linked events that eventually cause apoptosis [23]. ER plays a major role in protein synthesis, folding, assembly, transportation, and in maintaining Ca^{2+} homeostasis. In order to nullify the stress in ER lumen, cells elicit "ER stress response" or the "unfolded protein response" (UPR). In mammals, ER stress response consists of attenuation of protein synthesis to prevent protein accumulation and transcriptional induction of ER chaperone (e.g., glucose-regulated protein 78) and ERAD genes to increase folding capacity, enhance ERAD ability, and induce apoptosis to eliminate stressed cells [39]. ER stress may result as a consequence of various pathophysiological insults or by the alteration in Ca^{2+} homeostasis leading to the activation of three ER-localized transmembrane protein sensors. The three major transmembrane transducers that assist in UPR signaling cascade include RNA-dependent protein kinase-like ER kinase (PERK), activating transcription factor 6 (ATF6), and inositol-requiring ER-to-nucleus signal kinase 1 (IRE1). Glucose-regulated protein 78 (GRP78) and C/EBP homologous protein (CHOP) are two key proteins involved in the mechanism of ER stress. GRP78, a master regulator for ER stress, functions as a molecular chaperone and involves in the recognition of unfolded proteins [7]. GRP78 induces a protective mechanism during ER stress while CHOP is linked to trigger apoptosis. The up-regulation of proteins GRP78 and CHOP serves as an indicator of ER stress. ER stress is involved in various pathological conditions such as hypoxia [9], ischemia [25], viral infection [12], neurodegenerative disorders [36], and diabetes [41].

Although the association of oxalate toxicity and oxidative stress have been previously reported, oxalate-mediated ER stress response is yet to be elucidated. Therefore, the present study is focused to investigate the molecular interaction of oxalate with GRP78 in silico and to evaluate the ER stress-dependent and independent mechanism of oxalate-induced renal tubular cell apoptosis and kidney fibrosis. Further, to exclude the possibility that ER stress can occur up-stream of oxidative stress, *N*-acetylcysteine (NAC), an antioxidant that attenuates oxidative stress, is used.

Materials and methods

Molecular docking analysis of GRP78 protein with oxalate and calcium oxalate

The 3D-structure of GRP78 was constructed using homology modeling method, the same being unavailable in Protein Data Bank (PDB). For homology modeling, the sequence of GRP78 was retrieved from the NCBI protein sequence database and its corresponding template was identified using PSI-BLAST against the RCSB PDB. The 3D-structure was built using Swiss-Model server in template mode, with the aid of a PDB structure 3IUC as the template. Apparently, the rat GRP78 showed 99% identity and 58% query coverage to the template sequence 3IUC. The predicted model was validated using Swiss Model Assessment Server for structural validation using PROCHECK (http://swissmodel.expasy.org/) and Ramachandran plot. The optimized structure of GRP78 molecule was made to interact with oxalate and CaOx computationally using AUTODock. The 3D structures of oxalate and calcium oxalate was retrieved from PubChem (PubChem ID: CID 71081; CID 33005) available at https://pubchem.ncbi.nlm.nih.gov/. The docked complexes were visualized through PYMOL.

Cell culture and treatment

Normal rat kidney fibroblast-derived cell line (NRK49F) was procured from NCCS, India, and maintained in Dulbecco's modified Eagle medium (DMEM) supplemented with 10% fetal bovine serum (Hi-media), 100 U/ml penicillin (Hi-media), and 0.1 mg/ml streptomycin (Hi-media) and maintained at 37 °C in a humidified 5% CO_2 atmosphere. To evaluate the protective effect of NAC, NRK49F cells were simultaneously treated with oxalate and varying concentrations of NAC and the cell viability was evaluated by MTT assay. Following determination of the optimal concentration for both oxalate and NAC, cell lysates were analyzed for superoxide dismutase (SOD) activity [13], catalase (CAT) activity [34], and lipid peroxidation levels [26]. Mitochondrial mass was assessed by staining cells using 0.5 μM MitoTracker Deep Red (Invitrogen, Carlsbad, USA) and observed using Operetta High Content Imaging System (Perkin Elmer, USA). Level of net intracellular ROS production was detected by staining cells with 2,7-dichlorodihydrofluorescein diacetate (H_2DCFDA), a fluorescent probe and visualized using Nikon Eclipse Ti fluorescence microscope (Nikon, Tokyo, Japan). The early and late apoptotic cells were identified and quantified using annexin V-FITC/PI staining (BD Biosciences, USA).

Fluorescence detection of ER stress

The onset of ER stress in NRK49F cells exposed to oxalate overload was detected as described by Beriault et al. [1]. In brief, cells were cultured in 96-well plates and maintained overnight in a humidified atmosphere at 37 °C with 5% CO_2. Following incubation with oxalate for 18 h in the presence and absence of NAC, cells were washed with 1X phosphate-buffered saline (PBS) and incubated for 10 min with 5 μM of Thioflavin T (Sigma–Aldrich Inc. USA), before visualization. Fluorescent images of live cells were taken under a 10X objective with high content screening (Operetta High Content Imaging System, Perkin Elmer, USA).

Table 1 Primers used in the study

Gene	Sequence (5′–3′)
β- Actin	F-TTGCTGATCCACATCTGCTG R-GACAGGATGCAGAAGGAGAT
SOD	F-AAGGAGCAAGGTCGCTTACA R-ACACATCAATCCCCAGCAGT
CATALASE	F-GAATGGCTATGGCTCACACA R-CAAGTTTTTGATGCCCTGGT
GPX	F-TGCAATCAGTTCGGACATC R-CACCTCGCACTTCTCAAACA
GRP78	F-AACCCAGATGAGGCTGTAGCA R-ACATCAAGCAGAACCAGGTCAC
CHOP	F-CCAGCAGAGGTCACAAGCAC R-CGCACTGACCACTCTGTTTC
PERK	F-CTTTCGGTGCTCCAAGGCTC R-CGTATCCGATGTGGGAGCAA
IRE1	F-TGAGGGCAATGAGAAATAAGAAGC R-TGTAGGAGCAGGTGAGGGAAGC
ATF6	F-GATTGTGGGCGTCACTTCTCG R-TGGGATGCCAATGTTAGCCTG
TGF-β1	F-AAGAAGTCACCCGCGTGCTA R-TGTGTGATGTCTTTGGTTTTGTCA

Animals and treatments

Male Wistar rats (120–130 g) were divided into three groups (n = 6/group), and the experimental procedure was approved by the Internal Research and Review Board, Ethical Clearance, Biosafety and Animal Welfare Committee of Madurai Kamaraj University. Group I rats were fed with normal diet while groups II and III rats were fed with 5% potassium oxalate (KOx) containing pelleted diet (5% KOx mixed with normal rat chow before pelleting) for 42 days. From days 1 to 42, NAC (200 mg/kg body weight) was administered orally to group III rats. Animals were sacrificed at the end of the experimental period (day 42), and kidneys were excised for antioxidant profiling, gene expression studies, immunoblotting, and histopathological analysis.

RNA isolation and gene expression analysis

RNA was extracted with the single-step TRI Reagent (Sigma–Aldrich Inc. USA), and cDNA synthesis was performed with MMLV-reverse transcriptase. The relative quantitative gene expression levels of glutathione peroxidase (*GPx*), *SOD*, *CAT*, *β-actin*, *GRP78*, *CHOP*, *PERK*, *IRE1*, *ATF6*, and transforming growth factor ($TGF\text{-}\beta_1$) in NRK49F cells and kidney tissue were determined. The primers used in the study listed in Table 1 were selected from previous studies [11, 19, 20, 37].

Protein isolation and Western blot analysis

Cell homogenates were prepared for NRK49F cells and kidney tissue harvested from rats using a lysis buffer (Tris–Cl and

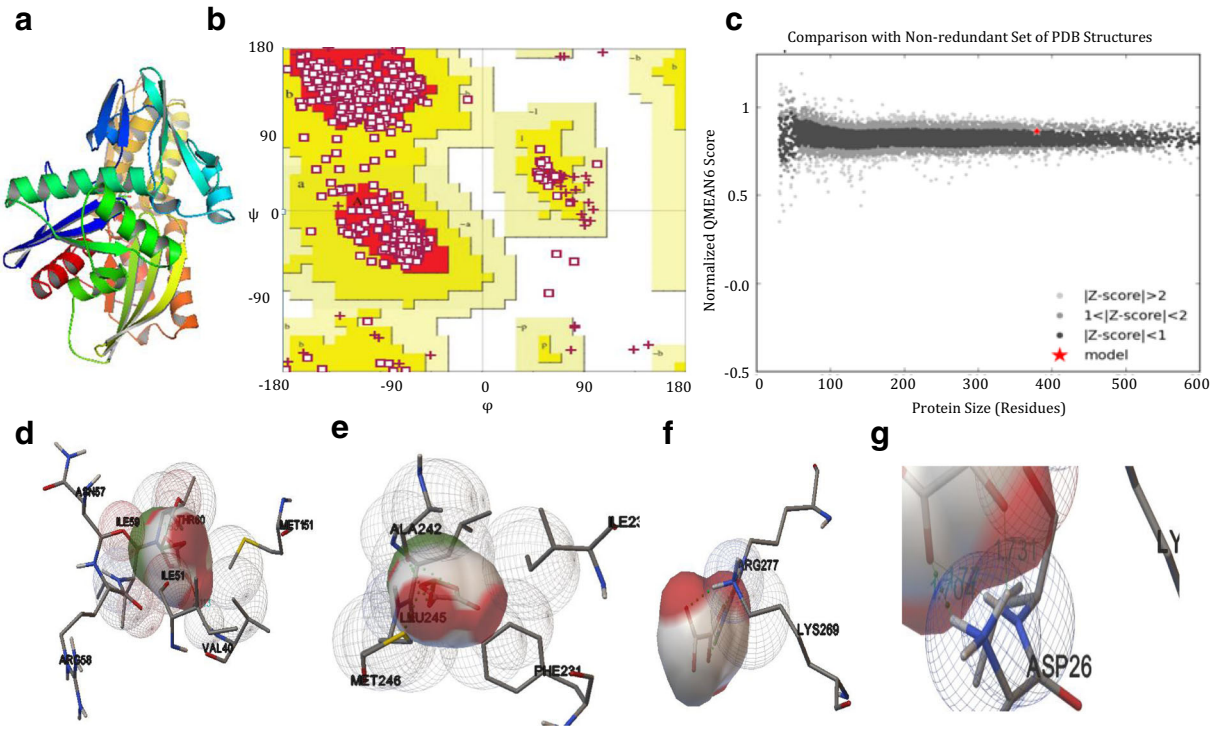

Fig. 1 **a** The homology-modeled target of GRP78 from *Rattus norvegicus*. **b** Ramachandran plot displays 98.6% amino acid residues have their torsion angles in the most favored region, 1.2% of amino acids in the allowed region, and 0.2% of having in the disallowed region. **c** The graphical representation of Z-score for *R. norvegicus* GRP78. The red star indicates the model which falls in the Z score < 1 region. **d**–**g** The protein 3D structures of human (3IUC) with calcium oxalate and oxalate as ligands and rat GRP78 with calcium oxalate and oxalate as ligands

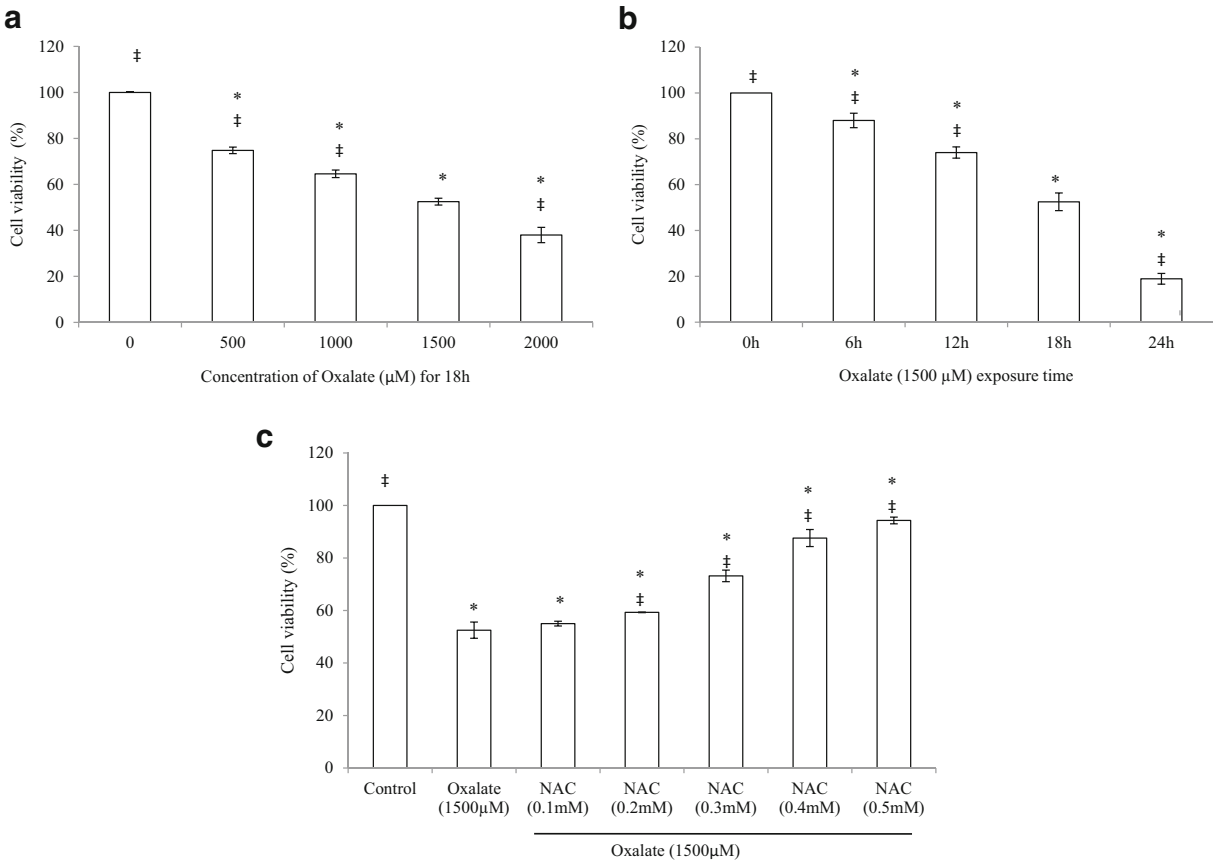

Fig. 2 Cytotoxic effect of KOx on cell viability and protective effect of NAC. **a** Dose-dependent effects of KOx:NRK49F cells treated with varying concentrations of KOx (0, 500, 1000, 1500, and 2000 μM) for 18 h. **b** Time-dependent effects of KOx:NRK49F cells treated with 1.5 mM KOx for 6, 12, 18, and 24 h. **c** Effect of *N*-acetylcysteine (NAC) on KOx-induced cell death. Cells were treated either alone with KOx (1.5 mM) or in combination with varying concentrations of NAC (0, 0.1, 0.2, 0.3, 0.4, and 0.5 mM). The data are mean value of three independent experiments. *Comparison with NRK49F cells devoid of oxalate stress. ‡Comparison with NRK49F cells exposed to oxalate stress (1500 μM for 18 h)

sodium fluoride, 50 mM of Tris–Cl; NAF, 10 mM; NaCl, 0.15 M; EDTA, 2 mM; sodium pyruvate, 1 mM; PMSF, 10 μg/ml; and Triton-X, 0.1%). The homogenate was centrifuged at 10,000 rpm for 10 min and the protein content was determined by Bradford assay (Sigma-Aldrich Inc. USA), calibrated with bovine serum albumin. Protein samples (30–

Table 2 The antioxidant profile of NRK49F cells and kidney homogenates

Antioxidant profile	NRK49F cells (No stress)	NRK49F cells (oxalate stress)	NRK49F cells (oxalate stress + NAC)
Catalase (μmol of H_2O_2 consumed/min/mg)	33.12 ± 1.55^{b}	18.21 ± 1.8^{a}	$29.09 \pm 2.77^{a,b}$
Superoxide dismutase (U/mg protein)	3.99 ± 0.32^{b}	1.72 ± 0.09^{a}	$2.91 \pm 0.18^{a,b}$
Lipid peroxidation (nmol/mg protein)	1.22 ± 0.09^{b}	3.66 ± 0.1^{a}	1.45 ± 0.04^{b}
	Group I (control)	Group II (5% KOx)	Group III (5% KOx + NAC)
Catalase (μmol of H_2O_2 consumed/min/mg)	62 ± 4.44^{d}	48 ± 3.52^{c}	60 ± 5.21^{d}
Superoxide dismutase (U/mg protein)	2.37 ± 0.22^{d}	1.47 ± 0.15^{c}	2.09 ± 0.51^{d}
Lipid peroxidation (nmol/mg protein)	1.2 ± 0.61^{d}	5 ± 0.9^{c}	$2 \pm 0.32^{c,d}$

The results are represented as mean ± SEM for six animals in each group. SOD—one enzyme unit was expressed as inverse of the amount of protein (mg) required for inhibiting reduction rate by 50% in 1 min. Values are statistically significant at $P < 0.05$

[a] Comparison with control NRK49F cells without oxalate stress

[b] Comparison with control NRK49F cells with oxalate stress

[c] Comparisons are made between Group I vs group II and III

[d] Comparisons are made between Group II vs Group I and III

40 μg) were resolved by SDS-PAGE and transferred to a PVDF membrane. The membranes were blocked in skim milk powder (5% *w*/*v*) with PBS containing 0.1% Tween 20 (PBS-T) for 1 h at room temperature and incubated with the respective primary antibodies anti-GRP78 antibody (1:1000 dilution, Santa Cruz - sc1051) and anti-CHOP antibody (1:1000 dilution, Santa cruz-sc575) at 4 °C overnight. Subsequently, the second antibody conjugated to HRP (1:1000 dilution, Santa Cruz) was used to incubate the membranes at room temperature for 2 h. Blots were detected using the enhanced chemiluminescence (ECL) western blotting reagents (GE healthcare Life Sciences, USA) and scanned using Bio-Rad Gel Doc XR; the intensity of protein bands normalized to β-actin (1:5000 dilution, Sigma-Aldrich Inc. USA) was quantified using Image Lab Software version 5 (Bio-Rad, USA).

Histopathological analysis

Specimens of kidney tissue were formalin fixed in 10% neutral-buffered formalin for histopathological analysis. Paraffin-embedded specimens were sectioned at 5 μm and subjected to hematoxylin and eosin staining for evaluation. Tubulointerstitial fibrosis was graded by degree of interstitial collagen deposition using Masson trichrome-stained sections of kidney tissue in a blinded fashion. Tubulointerstitial damage was scored on the basis 0 to 4+ (0 = no staining; 1 = <25% staining; 2 = 25 to < 50% staining; 3 = 50 to < 75% staining; 4 = 75 to 100%).

Statistical analysis

Each experiment was performed in triplicate and all values are represented as mean ± SEM. All the grouped data were statistically evaluated with SPSS Statistics software (version 19). Statistically significant differences between samples were determined by one-way ANOVA followed with post hoc analysis by least significant difference (LSD). For all comparisons, $P < 0.05$ was considered significant.

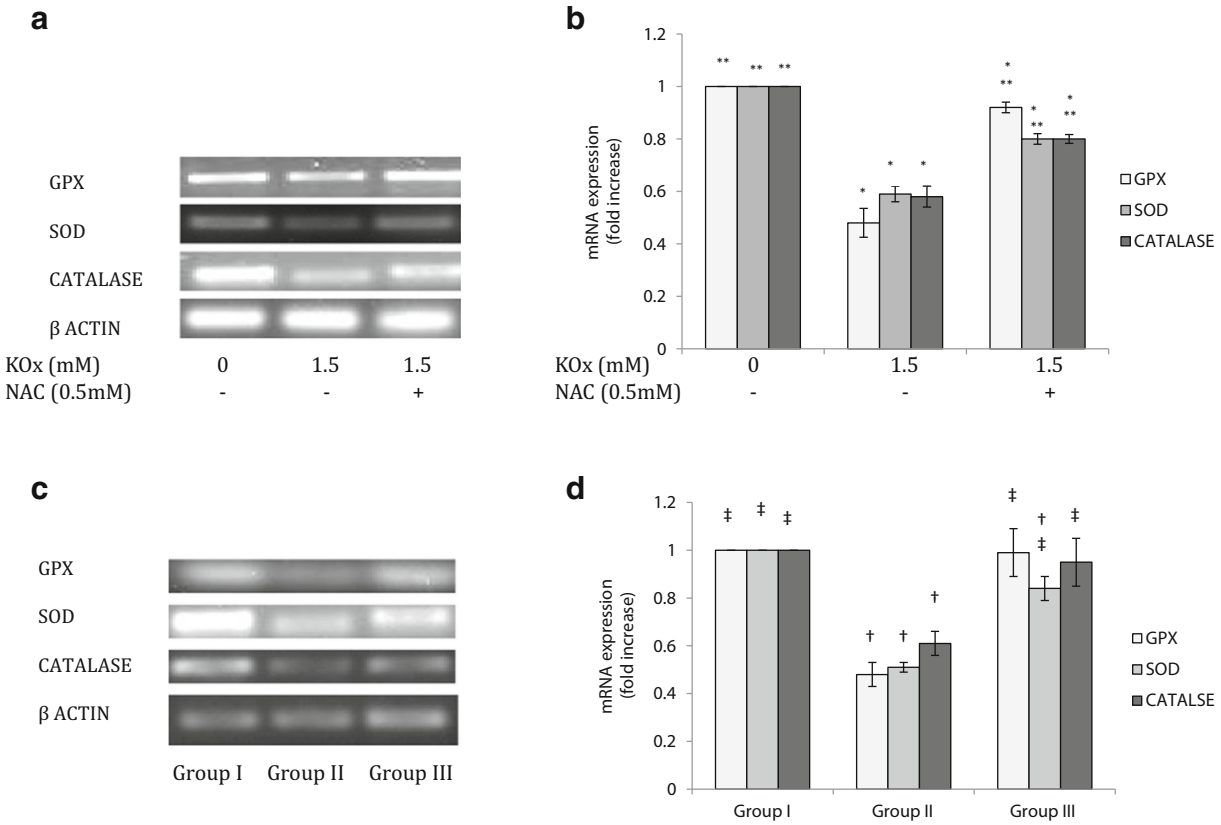

Fig. 3 Antioxidant profile analysis by semi-quantitative RT-PCR. **a** Representative photographs of semi-quantitative RT-PCR gel images for quantification of *GPX*, *SOD*, and *catalase* mRNA in NRK49F cells. **b** Bar diagram showing the relative change in mRNA expression level in NRK49F cells. **c** Representative photographs of semi-quantitative RT-PCR gel images for quantification of *GPX*, *SOD*, and *catalase* mRNA in experimental rats. **d** Bar diagram showing the relative change in mRNA expression level in experimental rats. *Comparison with NRK49F cells devoid of oxalate stress. **Comparison with NRK49F cells exposed to oxalate stress (1.5 mM for 18 h). †Comparison with group I rats. ‡Comparison with group II rats. The represented data are mean value of three independent experiments. Values are statistically significant at $P < 0.05$

Results

Interaction of oxalate and calcium oxalate with human and rat GRP78 protein

GRP78 is a major ER chaperone protein from Hsp70 protein family. The structure of rat GRP78 was not found in Protein Data Bank; hence, homology modeling was carried out using the FASTA sequence of *Rattus norvegicus* GRP78 obtained from NCBI (Accession no. NP_037215) database. A PDB BLAST search was done with GRP78 sequence which showed the PDB id 3IUC having the closest homology with 99% identity and 58% query coverage. The Ramachandran plot of the modeled protein documented the presence of 98.6% amino acids in the most favored region, 1.2% in the allowed region, and 0.2% in the disallowed region (Fig. 1a, b). The computed Z score value ranged between 0 and 1 which indicated the structure to be stereochemically stable (Fig. 1c). Molecular docking analyses of human (3IUC) and rat GRP78 with both oxalate and calcium oxalate showed efficient binding energy which is illustrated in Fig. 1d–g.

NAC treatment exerts protective effect against oxalate-induced damage

The optimal concentration of NAC against oxalate stress was determined by co-incubating different concentrations of NAC with oxalate. Supplementation of low concentrations of NAC

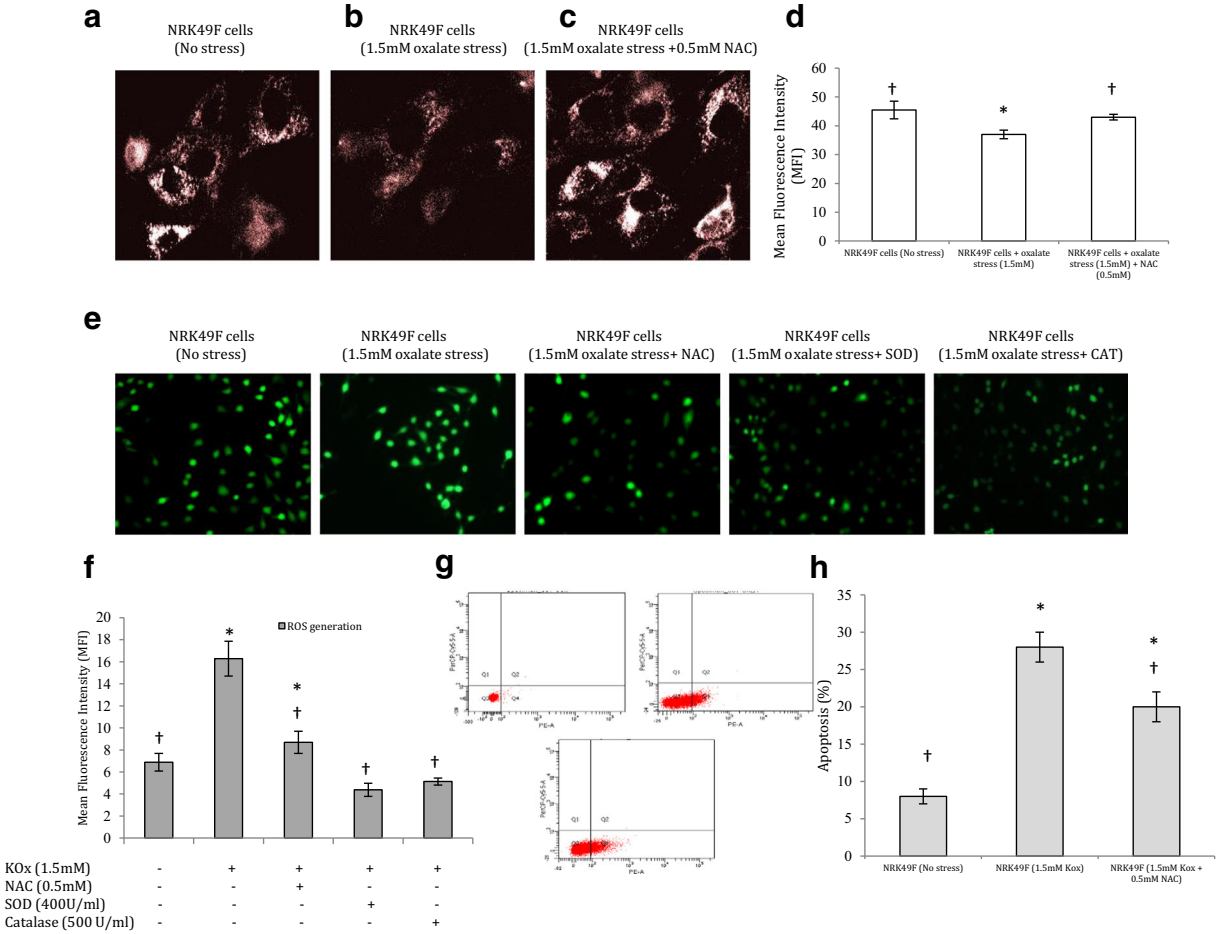

Fig. 4 Effect of NAC on mitochondrial membrane potential, ROS, and apoptosis in NRK49F cells exposed to oxalate stress. **a** The mitochondrial membrane potential ($\Delta\psi_m$)-sensitive fluorochrome MitoTracker Red in NRK49F cells devoid of oxalate stress. **b** NRK49F cells exposed to oxalate (1.5 mM). **c** NRK49F cells subjected to oxalate stress (1.5 mM) and NAC (0.5 mM). **d** Bar diagram depicting the quantification of Mito Tracker Red fluorescence intensity in KOx and KOx + NAC-treated NRK49F cells. **e** Representative images showing the inhibitory effect of NAC, catalase (CAT), and superoxide dismutase (SOD) on KOx-induced ROS generation. **f** Bar diagram shows the % fluorescence intensity of NRK49F cells following KOx and treatment with NAC, CAT, and SOD. **g** Representative histogram obtained by flow cytometry for detection of cell apoptosis AnnexinV-FITC/PI double staining. In each panel, lower left quadrant shows cells which are negative for both AnnexinV-FITC and PI; lower right shows Annexin V-positive cells which are in the early stage of apoptosis; upper left shows PI positive cells which are dead; and upper right shows both AnnexinV and PI positive, which are in the late stage of apoptosis. **h** Bar diagram showing the percentage of apoptotic cell populations. *Comparison with NRK49F cells (no stress) †Comparison with NRK49F cells exposed to oxalate stress (1.5 mM for 18 h). Each experiment was repeated a minimum of three independent times. Values are statistically significant at $P < 0.05$

(0.1 and 0.2 mM) showed minimal protective effect in oxalate-exposed (1.5 mM) cells, whereas 0.5 mM of NAC, significantly reversed damage in NRK49F cells (Fig. 2a–c). The dose of NAC (0.5 mM) that maintained a significant rise in cell viability (94.3 ± 2.3%) compared to KOx treatment alone was selected for further experiments. Oxidative stress, induced as a result of KOx stress, was effectively reduced by NAC supplementation. NAC intervention in NRK49F cells significantly restored the antioxidant enzyme activities of CAT (59.75%) and SOD (69.2%). In concordance with in vitro analysis, experimental rats administered with NAC showed significantly increased enzyme activities of CAT (25%) and SOD (42.18%) as represented in Table 2. Supplementation of KOx elevated lipid peroxidation levels by 3- and 4-fold in NRK49F cells and group II rats, respectively, while treatment with NAC attenuated lipid peroxidation activity. Gene expression analysis of *GPx*, *SOD*, and *catalase* showed significant down-regulation in oxalate-exposed cells and group II rats ($P < 0.05$) (Fig. 3). On the contrary, the antioxidant gene expression levels were up-regulated in the NAC-treated group (Fig. 3). The supplementation of NAC increased mitochondrial membrane potential (Fig. 4a–d) and significantly alleviated the levels of intracellular ROS generation close to that of untreated cells and cells treated with SOD and CAT (Fig. 4e–f). Interestingly, compared to untreated cells, a 1.5-fold increase in the population of cells that underwent early apoptosis was observed in NAC-treated cells (Fig. 4g, h), indicating oxalate-mediated apoptosis can occur independent of oxidative stress.

Oxalate exposure induces ER stress while NAC supplementation partially alleviates expression of GRP78 and CHOP in vitro and in vivo

The effect of ER stress in NRK49F cells was determined by Thioflavin T fluorescence assay. The ThT-fluorescence in NRK49F cells correlates directly with unfolded protein response activation [1]. Relative to control, fluorescence intensity was significantly increased in KOx treated cells (Fig. 5a–d). The KOx co-treatment of NRK49F cells with NAC partially decreased ThT fluorescence intensity (Fig. 5e, f), indicating that oxalate toxicity could induce ER stress independent of ROS generation. The results were confirmed by Real Time PCR which showed that oxalate stress significantly increased the up-regulation of endogenous ER stress markers GRP78 and CHOP. Real-time PCR and Western blot analysis indicates GRP78 and CHOP expression significantly up-regulated in a dose (0–1.5 mM) ($P < 0.05$)- and time-dependent manner (0–18 h) ($P < 0.05$). The expression of GRP78 and CHOP in NAC-treated NRK49F cells elevated moderately when compared to oxalate untreated cells (Fig. 6a–f). Similarly, the rats fed with 5% KOx diet showed an increased expression level of GRP78 and CHOP when compared to control. In concordance with in vitro results, the NAC-treated group III rats showed reduced expression of GRP78 and CHOP compared to the KOx-fed group II rats (Fig. 7a–c). The expression of GRP78 and CHOP protein detected by western blotting agreed with the gene expression data. Intervention with NAC partially attenuated the expression of GRP78 and CHOP in both in vitro and in vivo studies indicating that NAC treatment failed to fully restore ER stress.

Oxalate exposure triggered the expression of *PERK*, *IRE1*, and *ATF6* in vitro and in vivo

In an effort to study the downstream targets of UPR in oxalate-exposed NRK49F cells and experimental rat kidneys, mRNA levels of *PERK*, *IRE1*, and *ATF6* were analyzed. NRK49F cells subjected to oxalate stress showed significant ($P < 0.05$) up-regulation of *PERK*, *IRE1*, and *ATF6* (Fig. 8a). The in vivo data

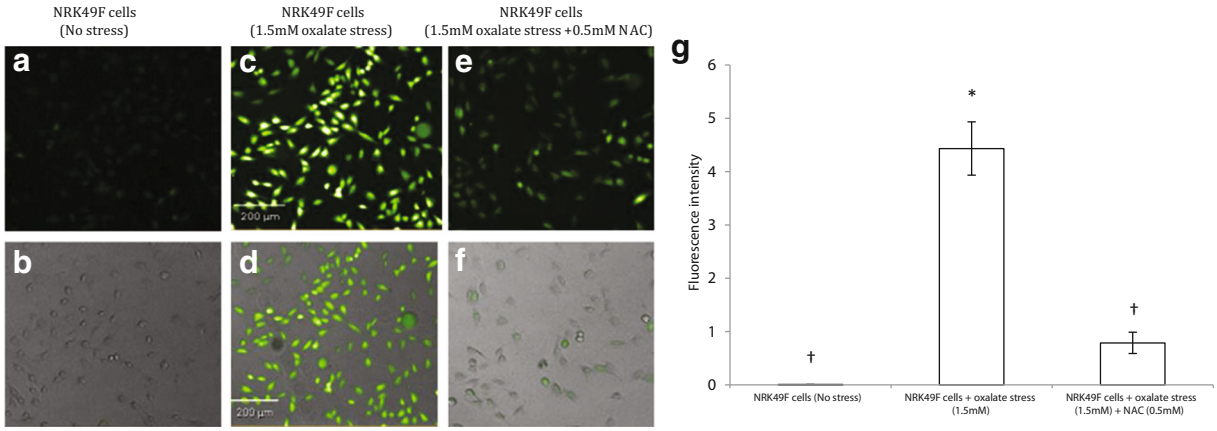

Fig. 5 ThT fluorescence intensity in relation to ER stress-induced activation of the unfolded protein response. NRK49F cells were treated with 1.5 mM KOx for 18 h in the absence and presence of 0.5 mM NAC. **a**, **b** Live cell images captured NRK49F cells not exposed to oxalate stress. **c**, **d** NRK49F cells exposed to oxalate stress (1.5 mM for 18 h). **e**, **f** NRK49F cells co-incubated with 1.5 mM of oxalate and 0.5 mM of NAC for 18 h. **g** Bar diagram ThT fluorescence intensity among cell populations. *Comparison with NRK49F cells (no stress). †Comparison with NRK49F cells exposed to oxalate stress (1.5 mM for 18 h). Each experiment was repeated a minimum of three independent times. Values are statistically significant at $P < 0.05$

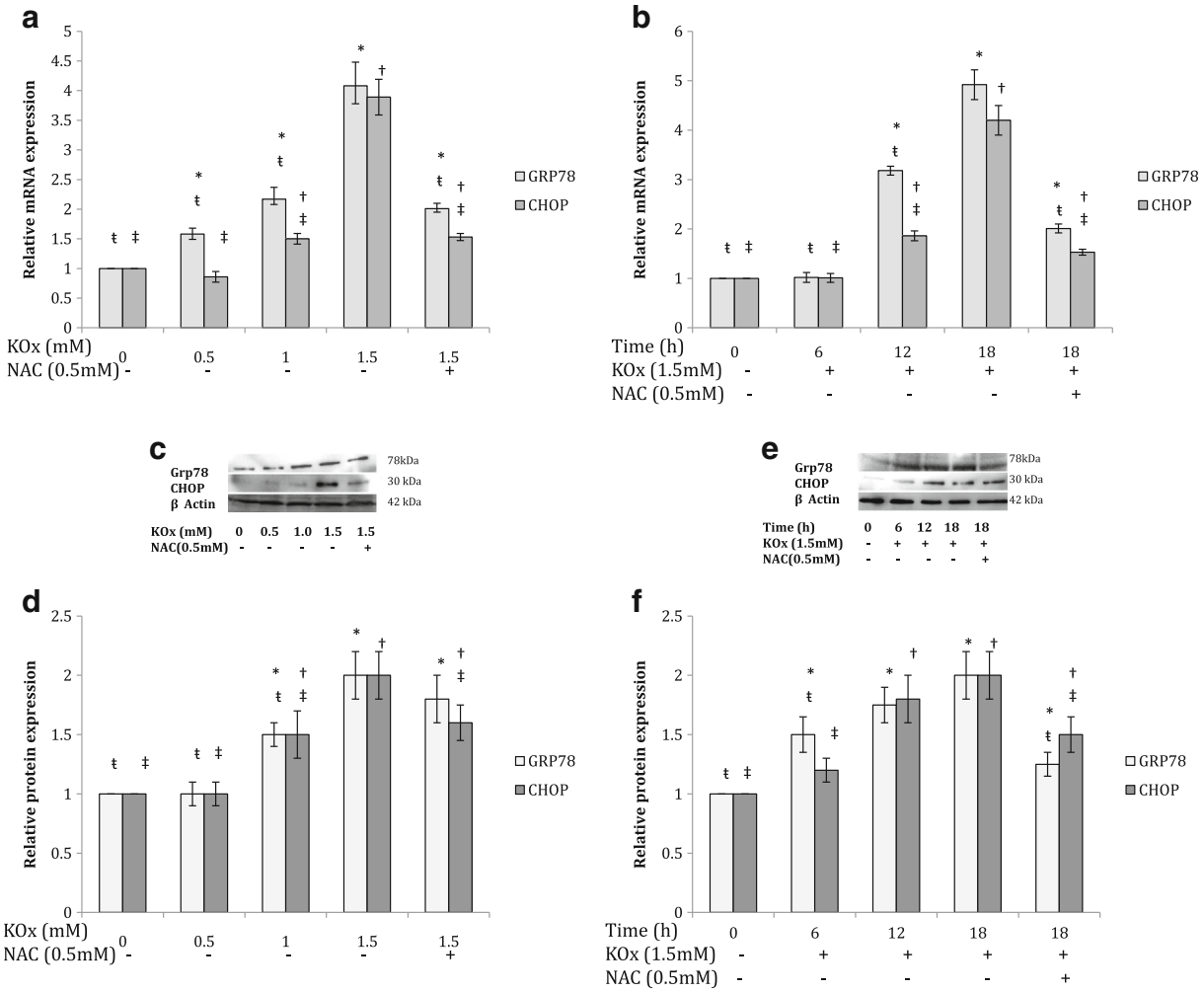

Fig. 6 Effect of ER stress markers GRP78 and CHOP exposed to KOx stress in NRK49F cells. **a** Relative gene expression of GRP78 and CHOP in a dose-dependent manner (0–1.5 mM KOx). **b** Relative gene expression of GRP78 and CHOP in time-dependent manner (0–18 h exposure of 1.5 mM KOx). Western blot analysis for GRP78 and CHOP expression. **c**, **d** Dose-dependent manner (0–1.5 mM KOx). **e**, **f** Time-dependent manner (0–18 h exposure of 1.5 mM KOx). *Comparison of GRP78 expression with NRK49F cells (no stress). †Comparison of CHOP expression with NRK49F cells (no stress). ŧComparison of GRP78 expression with NRK49F cells (1.5 mM oxalate stress for 18 h). ‡Comparison of CHOP expression with NRK49F cells (1.5 mM oxalate stress for 18 h). The level of individual bands was normalized by the level of β- actin and the representative band intensities. Data presented as ± S.E. Assays are performed in triplicates. Values are statistically significant at $P < 0.05$

agreed with the corresponding results obtained by in vitro studies (Fig. 8a). Interestingly, NAC treatment moderately alleviated the expression of all the three transmembrane transducers *PERK*, *IRE1*, and *ATF6* present in the ER ($P < 0.05$) (Fig. 8a, b). The results provide evidence that oxalate-induced apoptosis in NRK49F cells is mediated at least in part by ER stress.

Oxalate-mediated ER stress induce fibrotic remodeling in rat kidneys

In order to evaluate the role of oxalate-induced ER stress-mediated fibrosis in NRK49F cells and experimental rat kidneys, gene expression analysis of *TGF-β_1* was performed. A significant up-regulation of *TGF-β_1* was observed in both in vitro and in vivo (Fig. 9a, b). Histopathological analysis of kidney showed severe glomeruli damage, hemorrhage, and dilation of proximal tubules with interstitial inflammation in group II rats (Fig. 9d). The thickening of glomerular basement and the presence of fibrotic lesions (3+) were observed in group II rat kidneys (Fig. 9g). *N*-acetyl cysteine (NAC)-treated group III rats showed normal glomeruli with mild interstitial inflammation and fibrotic lesions (1+) (Fig. 9e, h). Control rat kidneys depicted normal glomeruli devoid of calcium oxalate (CaOX) crystal deposition and fibrotic lesions (Fig. 9c, f) (Table 3).

Discussion

Kidney stone disease is an increasingly prevalent systemic disorder with substantial health and economic consequences

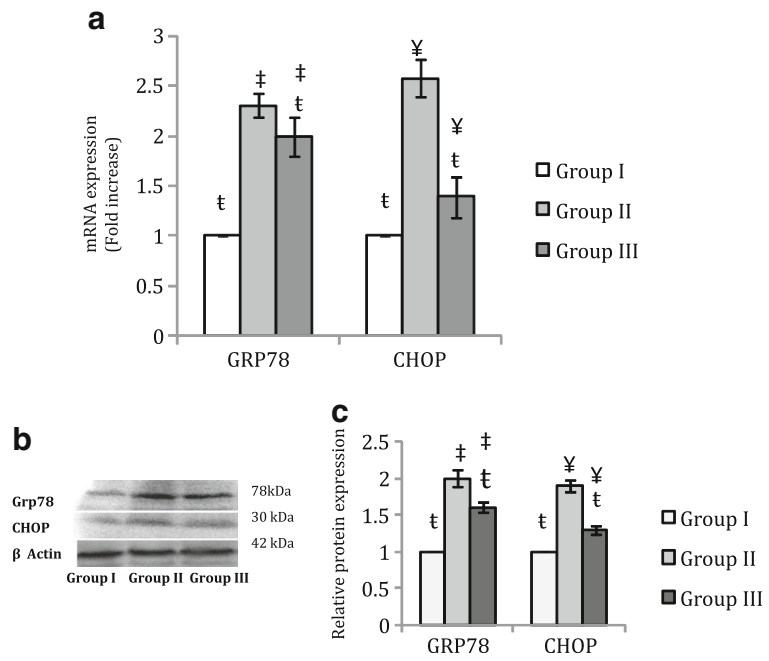

Fig. 7 Effect of ER stress markers GRP78 and CHOP in experimental rats. **a** Relative gene expression of GRP78 and CHOP in control and experimental rats on day 42. **b**, **c** Relative protein expression of GRP78 and CHOP in control and experimental rats on day 42. ‡Comparison of GRP78 expression with group I rats. ¥Comparison of CHOP expression with group I rats. ŦComparison of GRP78 and CHOP expression with group II rats. The level of individual bands was normalized by the level of β-actin and the representative band intensities. Data presented as ± S.E. Assays are performed in triplicates. Values are statistically significant at $P < 0.05$

[30]. Despite significant progress in understanding the pathophysiology of urolithiasis, the present therapeutic options have certain limitations. Previous reports have suggested a well established association between oxalate stress and ROS production that lead to oxidative stress in the physiology of kidney stone disease progression [8, 15]. Several metabolic disorders and heavy metal toxicity have a close involvement between oxidative stress and ER stress. However, the correlation between oxalate toxicity and ER stress is uncertain. Therefore, the present study is intended to elucidate the association of ROS and ER stress in oxalate-induced apoptosis.

Computational analysis of the rat GRP78 theoretical model revealed the ER stress response proteins efficiently interacts with oxalate and calcium oxalate that suggests oxalate can trigger an imbalance in ER homeostasis. Roop-ngam et al. [28] reported that oxalate binding with proteins such as catalase, mitochondrial NADH/ubiquinone oxidoreductase 51 kDa subunit, and GRP78 can result in the decreased activity of the protein thereby serving as modulators for kidney stone formation. In concordance with previous study [28], the results suggested that interaction of GRP78 with unfolded proteins was impaired in the presence of oxalate and CaOx resulting in the initiation of unfolded protein response (UPR).

Concordant with previous reports, antioxidant enzymes GPx, SOD, and catalase were modulated by the presence of oxalate whereas NAC treatment negated oxidative stress,

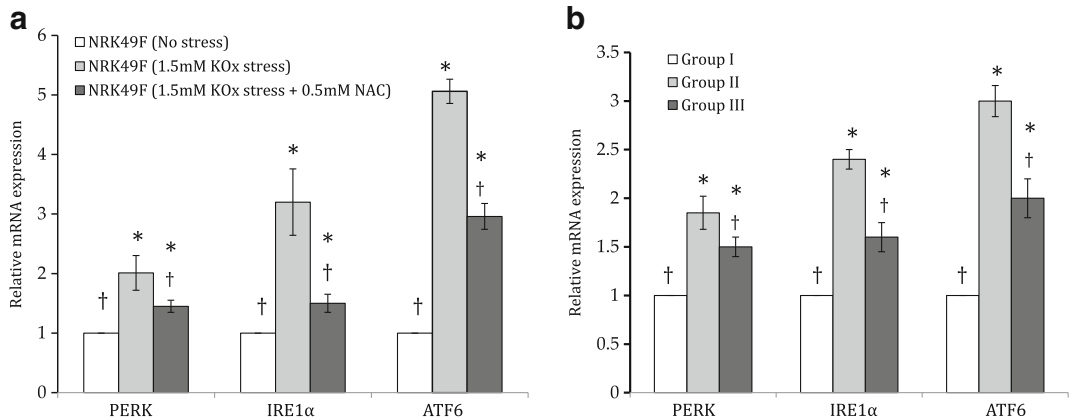

Fig. 8 Effect of ER stress markers PERK, IRE1α, and ATF6 in oxalate-exposed NRK49F cells and experimental rats. **a** Relative gene expression of PERK, IRE1α, and ATF6 in control and oxalate-exposed NRK49F cells. **b** Relative gene expression of PERK, IRE1α, and ATF6 in control and experimental rats on day 42. *Comparison of target genes PERK, IRE1α, and ATF6 expression with NRK49F cells (no stress) or group I rats. †Comparison of target genes PERK, IRE1α, and ATF6 expression with NRK49F cells (1.5 mM oxalate stress for 18 h) or group II rats. The level of individual bands was normalized by the level of β-actin and the representative band intensities. Data presented as ± S.E. Assays are performed in triplicates. Values are statistically significant at $P < 0.05$

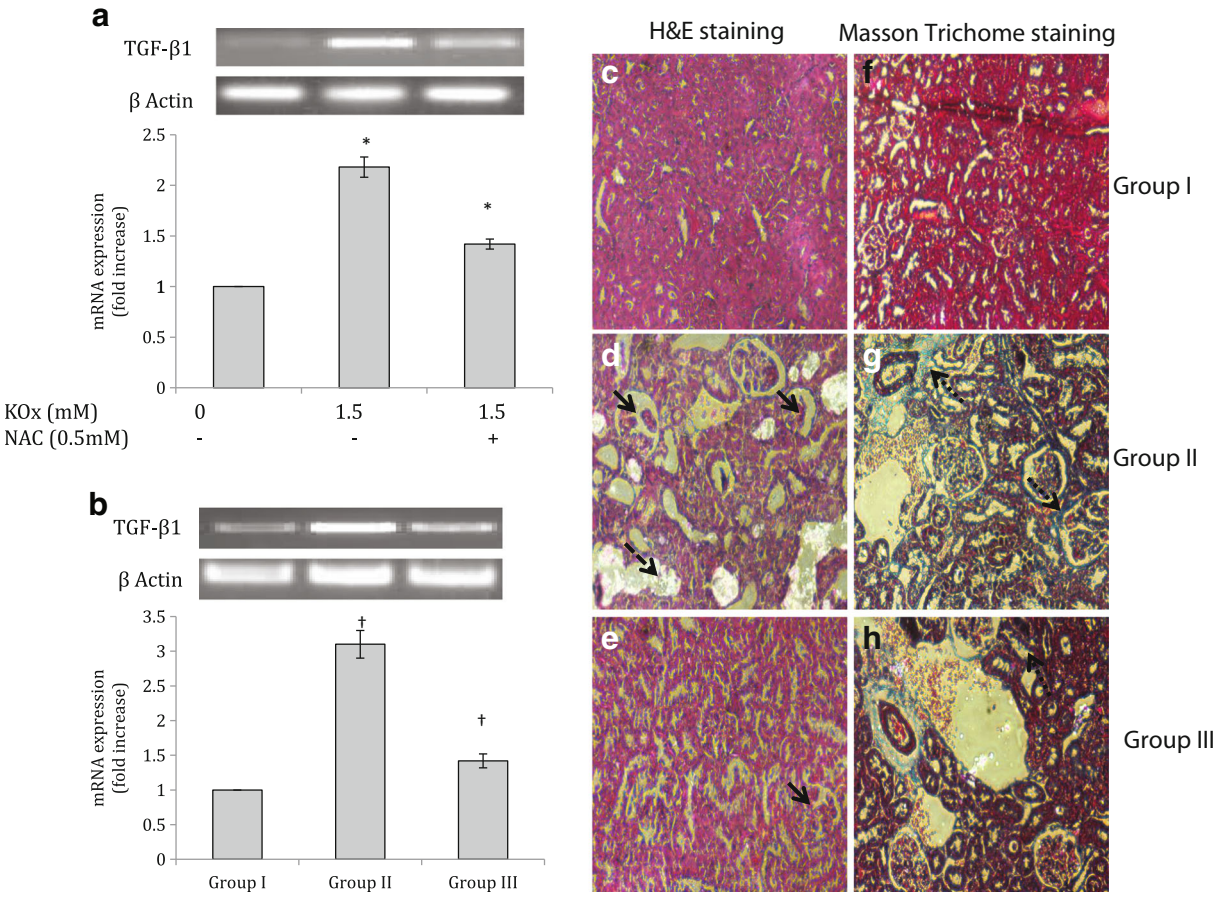

Fig. 9 Oxalate-mediated ER stress induce fibrotic remodeling. **a** Representative image of semi-quantitative RT-PCR gel images for quantification of TGF-β1 mRNA expression and bar diagram indicative of relative TGF-β1 mRNA expression in NRK49F. **b** Representative image of semi-quantitative RT-PCR gel images for quantification of TGF-β1 mRNA and bar diagram indicative of relative TGF-β1 mRNA expression in experimental rat kidneys. *Comparison with NRK49F cells devoid of oxalate stress. †Comparison with group I rat. **c** H&E-stained group I kidney sections exhibiting normal histology. **d** Group II sections demonstrating altered kidney histology. **e** Group III (NAC treated) kidney sections with moderate glomeruli atropy. **f** Masson's Trichrome-stained group I kidney sections exhibiting no fibrotic lesions. **g** Group II sections with high score (3+) for interstitial fibrosis. **h** Group III (NAC treated) kidney sections with minimal fibrotic lesions (1+). Solid black arrows depict damaged glomeruli. Dashed arrows represent crystal deposition. Round dot arrows indicate fibrotic lesions. Representative images captured using a × 40 objective magnification are shown

improved mitochondrial membrane potential, and restored the antioxidant profile [2, 22, 32]. NAC mitigates ROS production by up-regulating antioxidant systems, thus enhancing cell survival. NAC treatment promotes efficient renal functioning by reducing tubular dysfunction in group III rats. Oxalate stress increased lipid peroxidation in both NRK49F cells and experimental rat kidneys. Oxalate-induced apoptosis was markedly attenuated by administration of antioxidant NAC that indicates oxidative stress is the major mechanism for oxalate-induced apoptosis [5]. Although the supplementation of NAC attenuated ROS generation and significantly reversed apoptosis, the residual apoptosis can be attributed to ROS-independent mechanisms, possibly ER stress.

Various factors can hinder with ER function, causing accumulation of unfolded or misfolded proteins thereby leading to a cellular stress response. The role of ER stress in oxalate-induced renal tubular injury has not been extensively studied. Our results indicate a significant up-regulation of GRP78 at both gene and protein level that clearly implies the role of oxalate in the induction of ER stress. The results obtained were consistent with both in vitro and in vivo studies.

Table 3 A semi-quantitative analysis for histopathological alterations observed in hematoxylin-and-eosin-stained kidney sections of control and experimental rats

	Group I	Group II	Group III
Crystal deposition	0	4+	1+
Interstitial infiltration	0	3+	1+
Hemorrhage	1+	3+	2+
Glomerular atrophy	0	4+	2+
Inflammation	0	4+	2+

The severity of histopathological changes was scored on a scale 0 to 4+

Earlier studies have documented the involvement of ER stress in various pathological conditions [9, 12, 17, 25, 36, 41]. Reports have demonstrated that cadmium toxicity of renal tubular cells, lead toxicity in vascular endothelial cells, and fluorine toxicity of mouse ameloblast-derived cell line are influenced by ER stress [18, 33, 38]. Although ER stress is responsible for regulation of homeostasis mechanisms in ER, intense or persistent ER stress can induce programmed cell death or apoptosis. In the present study, the elevation of CHOP expression implicates that oxalate plays a key role in the process of ER stress-induced apoptosis and suggested that CHOP-mediated ER stress may be important for oxalate-induced renal injury. This result is concordant with previous study by Motin et al. [24] who reported that the altered pathophysiological properties can be due to the development of ER stress in nephrolithic kidneys. In addition to changes in general parameters, such as body weight, water intake, and urine excretion, the presence of oxalate in the microenvironment induces a significant decrease in urinary pH of experimental rats fed with oxalate diet compared to control group rats (data not shown). The acidic pH, a known stimulator for ER stress, may also prompt the activation of GRP78 and CHOP. Since Oyadomari et al. [27] reported that CHOP overexpression can create an imbalance in Ca^{2+} ion homeostasis, the up-regulation of CHOP in our study may prompt the release of Ca^{2+} ions that can act as a promoter for CaOx crystallization and aggregation. Detailed studies are needed to examine the release of Ca^{2+} ions and the binding of oxalate ions with calcium. Furthermore, the results of the present study revealed that ER stress induced by the accumulation of oxalate activates the UPR signaling cascade consisting of ER transmembrane protein sensors: PKR-like ER kinase (PERK), inositol-requiring protein1 (IRE1), and activating transcription factor 6 (ATF6). The IRE1 and ATF6 pathways have a pro-survival function but may mediate apoptosis under persistent ER stress [21, 40]. The significant increase in mRNA levels of IRE1, PERK, and ATF6 confirmed the role of ER stress in oxalate-mediated apoptosis.

Interestingly, NAC treatment in NRK49F cells completely inhibited oxidative stress but moderately reversed the level of ER stress markers and apoptosis, indicating a possibility that oxalate could also induce both ER stress and oxidative stress independently. In concordance with in vitro studies, oral administration of NAC fairly attenuated ER stress in experimental rats, indicative of oxalate inducing ER stress irrespective of oxidative stress. Similarly, Yokouchi et al. [38] elucidated the differential role of ROS in cadmium-induced ER stress apoptotic processes. Although Motin et al. [24] described the association between ER stress, oxidative damage, and nephrolithiasis, our current data indicated that oxalate induces apoptosis in renal fibroblast cells through ER stress-dependent and ER stress-independent mechanisms. The fact that oxalate-mediated apoptosis was markedly subdued by antioxidant treatment suggested that oxidative stress is the major mechanism for oxalate-induced apoptosis.

During stone formation, macrophages are known to penetrate the renal interstitium around crystal deposits resulting in the stimulation of renin-angiotensin system, ROS generation, ECM production, and fibrosis [2, 16]. In concordance with previous literature, the present study revealed the up-regulation of *TGF-β_1* in renal fibroblast cells and kidney tissue when exposed to oxalate overload [14, 35]. NRK-49F renal fibroblasts cells, an in vitro model, have been extensively used in fibrogenesis studies, especially those induced by TGF-β [10, 29, 32]. Furthermore, Umekawa et al. [35] suggested that on oxalate exposure, TGF-β promotes the transformation of renal fibroblast cells to myofibroblasts resulting in renal fibrosis. Based on the previous literature, in this study, NRK-49F cell type was chosen as a model to establish the role of hyperoxaluria and ER stress in tubulointerstitial fibrosis. Interestingly, a significant up-regulation in *TGF-β_1* expression was observed in NRK49F cells co-treated with both oxalate

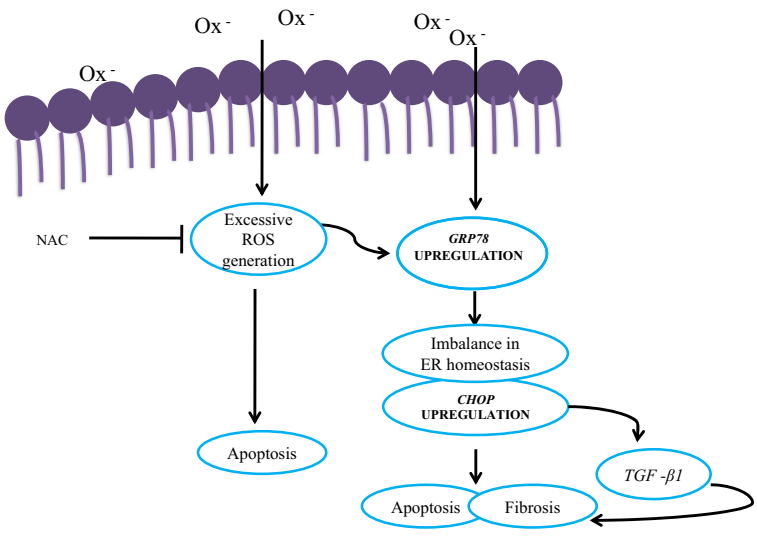

Fig. 10 Illustration of the mechanisms by which oxalate may induce apoptosis in the pathogenesis of CaOx stone disease

and NAC when compared to cells not exposed to oxalate stress. Moreover, the onset of renal fibrosis in kidneys of group II and III rats was further established by Trichrome Masson staining by in vivo studies. Earlier reports have demonstrated the involvement of ER stress in fibrotic remodeling and epithelial-to-mesenchymal transformation in human proximal tubule cells [3, 6]. The results of the present study suggested that besides oxalate-mediated oxidative stress, ER stress could also play a pivotal role in the progression of renal fibrosis when subjected to oxalate toxicity. Since UPR mechanisms have been implicated in various disease conditions, it is essential to identify the components of ER stress that respond to treatment options. Therefore, attenuating ER stress may pave the way for prevention of renal fibrosis and serve as a potential therapeutic target in CaOx stone disease.

The results demonstrated that ER stress can mediate the pathogenesis of oxalate-induced apoptosis and renal fibrosis (Fig. 10). The data also provides evidence that oxidative stress is mainly responsible for downstream of ER stress and illustrate important signaling events involved with the association of ER stress and oxalate toxicity in the development of urolithiasis. Further studies are required to evaluate the selective involvement of ROS in oxalate-mediated ER stress-dependent pro-apoptotic pathways.

Acknowledgements This work was supported by University Grants Commission (UGC), and IPLS program, Department of Biotechnology (DBT), New Delhi, India. The authors also thank UGC-CEGS, UGC-CAS, UGC-NRCBS, DST-FIST, and DST-PURSE program for the central instrumentation facility at SBS, MKU.

Compliance with ethical standards The experimental procedure was approved by the Internal Research and Review Board, Ethical Clearance, Biosafety and Animal Welfare Committee of Madurai Kamaraj University.

Conflict of interest The authors declare that they have no conflicts of interest.

References

1. Beriault DR, Werstuck GH (2013) Detection and quantification of endoplasmic reticulum stress in living cells using the fluorescent compound Thioflavin T. Biochim Biophys Acta 1833:2293–2301
2. Cao LC, Honeyman TW, Cooney R (2004) Mitochondrial dysfunction is a primary event in renal cell oxalate toxicity. Kidney Int 66: 1890–1900
3. Chiang CK, Hsu SP, Wu CT, Huang JW, Cheng HT, Chang YW, Hung KY, Wu KD, Liu SH (2011) Endoplasmic reticulum stress implicated in the development of renal fibrosis. Mol Med 17:1295–1305
4. Chiangjong W, Thongboonkerd V (2016) Calcium oxalate crystals increased enolase-1 secretion from renal tubular cells that subsequently enhanced crystal and monocyte invasion through renal interstitium. Sci Rep 6:24064
5. Davalos M, Konno S, Eshghi M, Choudhury M (2010) Oxidative renal cell injury induced by calcium oxalate crystal and renoprotection with antioxidants: a possible role of oxidative stress in nephrolithiasis. J Endourol 24:339–345
6. Dickhout JG, Carlisle RE, Austin RC (2011) Interrelationship between cardiac hypertrophy heart failure and chronic kidney disease endoplasmic reticulum stress as a mediator of pathogenesis. Circ Res 108:629–642
7. Ding W, Yang L, Zhang M, Gu Y (2012) Reactive oxygen species-mediated endoplasmic reticulum stress contributes to aldosterone-induced apoptosis in tubular epithelial cells. Biochem Biophys Res Commun 418:451–456
8. Farooq SM, Boppana NB, Asokan D, Sekaran SD, Shankar EM, Li C, Gopal K, Bakar SA, Karthik HS, Ebrahim AS (2014) C-phycocyanin confers protection against oxalate-mediated oxidative stress and mitochondrial dysfunctions in MDCK cells. PLoS One 9: e103361
9. Feldman DE, Chauhan V, Koong AC (2005) The unfolded protein response: a novel component of the hypoxic stress response in tumors. Mol Cancer Res 3:597–605
10. Grotendorst GR, Rahmanie H, Duncan MR (2004) Combinatorial signaling pathways determine fibroblast proliferation and myofibroblast differentiation. FASEB J 18:469–479
11. Guo F, Yue H, Wang L, Ding C, Wu L, Wu Y, Gao F, Qin G (2017) Vitamin D supplement ameliorates hippocampal metabolism in diabetic rats. Biochem Biophys Res Commun 490:239–246
12. He B (2006) Viruses endoplasmic reticulum stress and interferon responses. Cell Death Differ 13:393–403
13. Kakkar P, Das B, Viswanathan PN (1984) A modified spectrophotometric assay of superoxide dismutase. Indian J Biochem Biophys 21:130–132
14. Kanlaya R, Sintiprungrat K, Thongboonkerd V (2013) Secreted products of macrophages exposed to calcium oxalate crystals induce epithelial mesenchymal transition of renal tubular cells via RhoA-dependent TGF-β1 pathway. Cell Biochem Biophys 67: 1207–1215
15. Khan SR (2004) Role of renal epithelial cells in the initiation of calcium oxalate stones. Nephron Exp Nephrol 98:e55–e60
16. Khan SR (2014) Reactive oxygen species inflammation and calcium oxalate nephrolithiasis. Transl Androl Urol 3:256–276
17. Kim I, Xu W, Reed JC (2008) Cell death and endoplasmic reticulum stress: disease relevance and therapeutic opportunities. Nat Rev Drug Discov 7:1013–1030
18. Kubota K, Lee DH, Tsuchiya M, Young CS, Everett ET, Martinez-Mier EA, Snead ML, Nguyen L, Urano F (2005) Fluoride induces endoplasmic reticulum stress in ameloblast responsible for dental enamel formation. J Biol Chem 280:23194–23202
19. Ling Q, Yu X, Wang T, Wang SG, Ye ZQ, Liu JH (2017) Roles of the exogenous H2S-mediated SR-A signaling pathway in renal ischemia/ reperfusion injury in regulating endoplasmic reticulum stress-induced autophagy in a rat model. Cell Physiol Biochem 41:2461–2474
20. Liu G, Sun Y, Li Z, Song T, Wang H, Zhang Y, Ge Z (2008) Apoptosis induced by endoplasmic reticulum stress involved in diabetic kidney disease. Biochem Biophys Res Commun 370: 651–656
21. Logue SE, Cleary P, Saveljeva S, Samali A (2013) New directions in ER stress-induced cell death. Apoptosis 18:537–546
22. Mahmoodi M, Mehranjani SM, Shariatzadeh SM, Eimani H, Shahverdi A (2015) N-acetylcysteine improves function and follicular survival in mice ovarian grafts through inhibition of oxidative stress. Reprod BioMed Online 30:101–110
23. Malhotra JD, Kaufman RJ (2007) Endoplasmic reticulum stress and oxidative stress: a vicious cycle or a double-edged sword? Antioxid Redox Signal 9:2277–2293
24. Motin YG, Lepilov AV, Bgatova NP, Zharikov AY, Motina NV, Lapii GA, Lushnikova EL, Nepomnyashchikh LM (2016)

Development of endoplasmic reticulum stress during experimental oxalate nephrolithiasis. Bull Exp Biol Med 160:381–385
25. Nakka VP, Gusain A, Raghubir R (2010) Endoplasmic reticulum stress plays critical role in brain damage after cerebral ischemia/reperfusion in rats. Neurotox Res 17:189–202
26. Ohkawa H, Ohishi N, Yagi K (1979) Assay for lipid peroxides in animal tissues by thiobarbituric acid reaction. Anal Biochem 95: 351–358
27. Oyadomari S, Mori M (2004) Roles of CHOP/GADD153 in endoplasmic reticulum stress. Cell Death Differ 11:381–389
28. Roop-ngam P, Chaiyarit S, Pongsaku N, Thongboonkerd V (2012) Isolation and characterizations of oxalate-binding proteins in the kidney. Biochem Biophys Res Commun 424:629–634
29. Roberts AB, Sporn MB, Assoian RK, Smith JM, Roche NS, Wakefield LM, Heine UI, Liotta LA, Falanga V, Kehrl JH, Fauci AS (1986) Transforming growth factor type β: rapid induction of fibrosis and angiogenesis *in vivo* and stimulation of collagen formation *in vitro*. Proc Natl Acad Sci U S A 83:4167–4171
30. Sakhaee K, Maalorf NM, Sinmott B (2012) Kidney stones 2012: pathogenesis diagnosis and management. J Clin Endocrinol 97: 1847–1860
31. Scales CD Jr, Smith AC, Hanley JM, Saigal CS (2012) Urologic diseases in America project. Prevalence of kidney stones in the United States. Eur Urol 62:160–165
32. Shen Y, Miao NJ, Xu JL, Gan XX, Xu D, Zhou L, Xue H, Zhang W, Lu LM (2016) N-acetylcysteine alleviates angiotensin II-mediated renal fibrosis in mouse obstructed kidneys. Acta Pharmacol Sin 37: 637–644
33. Shinkai Y, Yamamoto C, Kaji T (2010) Lead induces the expression of endoplasmic reticulum chaperones GRP78 and GRP94 in vascular endothelial cells via the JNK-AP-1 pathway. Toxicol Sci 114: 378–386
34. Sinha K (1972) Colorometric assay of catalase. Anal Biochem 47: 389–394
35. Umekawa T, Iguchi M, Uemura H (2006) Oxalate ions and calcium oxalate crystal-induced up-regulation of osteopontin and monocyte chemoattractant protein-1 in renal fibroblasts. BJU Int 98:656–660
36. Viana RJ, Nunes AF, Rodrigues CM (2012) Endoplasmic reticulum enrollment in Alzheimer's disease. Mol Neurobiol 46:522–534
37. Wang Z, Shah SV, Liu H, Baliga R (2014) Inhibition of cytochrome P450 2E1 and activation of transcription factor Nrf2 are renoprotective in myoglobinuric acute kidney injury. Kidney Int 86:338–349
38. Yokouchi M, Hiramatsu N, Hayakawa K, Okamura M, Du S, Kasai A (2008) Involvement of selective reactive oxygen species upstream of proapoptotic branches of unfolded protein response. J Biol Chem 283:4252–4260
39. Yoshida H (2007) ER stress and diseases. FEBS J 274:630–658
40. Yoshida H, Okada T, Haze K, Yanagi H, Yura T, Negishi M, Mori K (2000) ATF6 activated by proteolysis binds in the presence of NF-Y (CBF) directly to the cis-acting element responsible for the mammalian unfolded protein response. Mol Cell Biol 20:6755–6767
41. Zhang N, Cao MM, Liu H, Xie GY, Li YB (2015) Autophagy regulates insulin resistance following endoplasmic reticulum stress in diabetes. J Physiol Biochem 71:319–327